Quantitative imaging with fast fan-beam scan using a benchtop X-ray fluorescence computed tomography

Liang Li*, Siyuan Zhang, Ruizhe Li, Zhiqiang Chen

***Abstract*—X-ray fluorescence computed tomography (XFCT) is a quantitative imaging technique which detects the characteristic X-ray photons from certain elements stimulated by an excitation source. Hence, it can reconstructs the two- (2D) or three-dimensional (3D) distribution of nonradioactive high atomic nanoparticles (NPs) within an organism, such as gold, gadolinium, and iodine. However, early XFCT performed on a high-intensity monochromatic synchrotron source with large facilities or a pencil beam collimated from a polychromatic X-ray tube with a very long scanning time. In this paper, we developed a fast full-field fan-beam XFCT on our SKYFI (simultaneous K-edge and X-ray fluorescence CT imaging) benchtop setting with a conventional low-intensity polychromatic X-ray tube, energy-sensitive photon-counting detector arrays and a tungsten pinhole collimator. A homemade phantom that contained gadolinium solutions was scanned for 30 min using a full-field fan-beam in the third-generation CT geometry. After accurate detector energy calibration, scattering and attenuation corrections, experimental results showed high sensitivity and accuracy. Therefore, this kind of full-field XFCT identifies a clear path toward for biomedical imaging of exogenous molecular NP probes.**

***Index Terms*—X-ray fluorescence, computed tomography, nanoparticle (NP), image reconstruction, photon-counting detector.**

I. Introduction

X-RAY CT is becoming widely used in various applications, e.g., biomedical imaging, industrial imaging and security inspection. Essentially, X-ray CT including spectral CT utilizes the attenuation information of X-ray photons passing through the different body tissues. Because these attenuation contrasts of different biological tissues are not prominent, it is difficult to accurately identify a diseased tissue or target materials due to a high-level background [1-3]. Different from the traditional X-ray CT as well as spectral CT, X-ray fluorescence computed tomography (XFCT) detects the characteristic X-ray photons, i.e., X-ray fluorescence (XRF), from certain elements excited by initial X-rays. It is a quantitative imaging modality reconstructing the 2D or 3D distributions of nonradioactive high atomic nanoparticle (NP) probes within an organism, such as gold, gadolinium, and iodine [4-6]. Because XFCT belongs to stimulated emission imaging, the NP contrast in XFCT images is independent from the surrounding tissue, which is the biggest advantage comparing to traditional X-ray CT as well as spectral CT [7-8]. Therefore, XFCT has a great potential in high sensitivity molecular imaging [9].

XRF element analysis has a very long history of use for many applications including healthcare. To the best of our knowledge, the XRF tomographic device was proposed by Boisseau et al. in 1989 [10]. In order to reduce the signal background, early XFCT experimental systems generally utilized monochromatic X-ray source to excite the XRF signals, e.g., high-intensity synchrotron radiation sources with very large facilities [11-17]. However, the high-cost and low- practicality limits the use of a synchrotron for biomedical imaging applications. Therefore, in recent years the use of a conventional polychromatic X-ray tube has become the mainstream of XFCT research [18-20]. In order to characterize each XRF line, most of the published papers chose a pencil beam collimated from a polychromatic X-ray tube or an energy-resolved detector [21-26]. Thus, their XFCT acquisitions have been performed in a first generation CT geometry, i.e., rotation-and-translation, which acquired a very long scanning time, e.g., 279 min [27]. A design of fan-beam XFCT system was proposed by Cong et al., but it needed large detectors and complicated collimators [28].

For fast and superior XFCT imaging, we developed a simultaneous K-edge and X-ray fluorescence CT imaging (SKYFI) experimental setup which includes a conventional low-intensity polychromatic X-ray tube, two separate photon counting detector arrays, a pin-hole collimator and a rotation stage [29]. This paper reports our latest full-field fan-beam XFCT experimental results of a homemade phantom that contained gadolinium solutions. Using the third-generation CT geometry, the phantom was only scanned for 30 min, which was also the shortest data acquisition time in the published papers. After accurate detector energy calibration, scattering and attenuation corrections, these experimental results showed high sensitivity and accuracy.

Manuscript received January 16, 2017. This work was partially supported by the grants from NSFC 61571256, 81427803, and 11525521, and the Beijing Municipal Science and Technology Commission (Z151100003915079).

Liang Li, Siyuan Zhang, Ruizhe Li and Zhiqiang Chen are all with Department of Engineering Physics, Tsinghua University, Beijing, 100084, China & Key Laboratory of Particle & Radiation Imaging (Tsinghua University), Ministry of Education, 100084, China.

Corresponding author: Liang Li, lliang@tsinghua.edu.cn

DOI: 10.12059/Fully3D.2017-11-3108006

II. SYSTEM AND METHOD

A. The SKYFI system

Because the XRF and K-edge properties of an element are physically complementary, the SKYFI experimental setup simultaneously acquired XRF and K-edge signals in a single CT scan from one or more contrast agents (e.g., iodine, gadolinium, gold NPs) which represent the attenuation and fluorescence information from the same physical process of photoelectric absorption, respectively. The most advantage of SKYFI is that the information of K-edge CT can be used for accurately real-time attenuation correction of XFCT. Thus, SKYFI can provide superior concentration accuracy of the contrast agents.

Fig. 1 is a schematic diagram of the SKYFI experimental setup. It includes a conventional cone-beam X-ray tube, a pin-hole collimator and two separate photon counting detector arrays which are placed in a nearly right angle. The pin-hole collimator in front of the XFCT detector makes the full-field fan-beam XFCT imaging in one rotation scan possible.

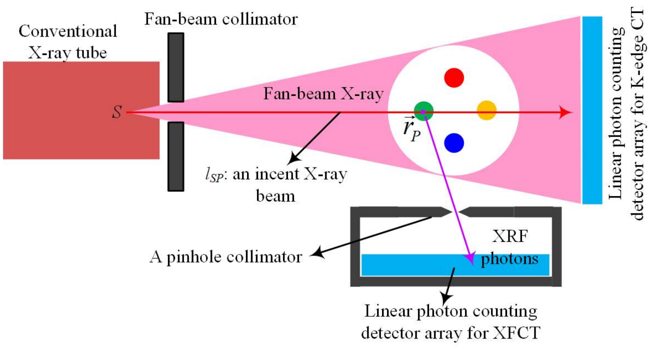

Fig.1. Schematic diagram of the SKYFI experimental setup

B. Calibration methods

Calibrations are very important procedures in high sensitivity XFCT imaging, which mainly include three kinds of methods: energy calibration of photon-counting detector, scattering photon correction, and XRF attenuation correction.

Energy calibration is an essential procedure of photon-counting detector which allows the connection between detector output and actual energy, and aligns the uniformity of thresholds and pixels. Especially for XFCT imaging, accurate detector configuration of energy thresholds is the most critical factor in order to reduce the background or improve the contrast-to-noise ratio (CNR). Usually, energy calibration can be realized using synchrotron monochromatic illumination, radioactive isotopes, X-ray kilovoltage peaks (kVp), and XRF method. We developed a feasible energy calibration for multi-threshold photon-counting detectors based on reconstructed XRF spectra [29].

Usually, the relation between detector response and the actual photon energy can be described with the linear model in the linear range of the charge sensitive amplifier

$$E = kD + b\,, \tag{1}$$

where E and D are the photon energy and detector output, respectively. The energy calibration is to determine the coefficients k and b for different pixels and different electronics settings (e.g., peaking time and gain). The XRF method with a double threshold scan mode was used to complete energy calibration, which was proved to be superior to single threshold scan mode and the kVp method.

The other two important influences on XFCT image quality are the interference of Compton scattering of the incident polychromatic X-ray beam, and the attenuation (absorption) effect of the XRF photons passing through the scanned object. The scattering background can be measured by the different energy bins of the photon-counting detector or estimated by the Klein-Nishina function from the K-edge CT images. This paper used the former method. As mentioned, the accurate attenuation map of XRF photons can be also provided by the simultaneous K-edge CT image at the corresponding energy-bin.

C. Imaging model and reconstruction algorithm of XFCT

The physics and signal model of XFCT are well known. Because XRF photons are the emissions from contrast agents excited by initial X-rays, its imaging models include three parts: 1) the attenuation model of the incident X-ray beam arriving at any position $\vec{r}_P$ from the X-ray tube; 2) XRF generation model when incident X-ray beam interacts with contrast agents; and 3) attenuation and collection model of the XRF photons emitted from position P travel through the object.

As showed in Fig.1, the incident X-ray photons arriving at $\vec{r}_P$ can be expressed as

$$I\left(E,\vec{r}_P\right) = I_0\left(E\right)\cdot e^{-\int_{l_{SP}(\vec{r})}\mu(E,\vec{r})d\vec{r}} \tag{1}$$

where l_{SP} means the X-ray path from the X-ray source to $\vec{r}_P$. $I_0\left(E\right)$ is the incident photon counts at energy E .

The XRF photons generated from $\vec{r}_P$ can be expressed as

$$I_{XRF}\left(\vec{r}_P\right) = \int_{E_K}^{E_{\max}} I\left(E,\vec{r}_P\right)\cdot\omega\cdot\rho\left(\vec{r}_P\right)\cdot\mu_{pe}^{m}(E)dE \tag{2}$$

where $\mu_{pe}^{m}(E)$ is the photoelectric mass absorption coefficient of the contrast agent, ω is the yield of fluorescence X-rays which can be approximated as a constant. $\rho\left(\vec{r}_P\right)$ is the concentration of contrast agent at $\vec{r}_P$ represented as a weight percent. At last, the emitted monochromatic XRF photons arriving into a perfect photon counting detector can be expressed as,

$$I_{DXF} = \int_{l_P} I_{XRF}\left(\vec{r}_P\right)\cdot\int_{Ang} e^{-\int_{l_{PD}(\vec{r})}\mu_{XRF}(\vec{r})d\vec{r}}\, d\gamma d\vec{r}_P \tag{3}$$

where $l_{PD}(\vec{r})$ means the XRF path starting from $\vec{r}_P$ to the detector and passing the pin-hole collimator. $\mu_{XRF}\left(\vec{r}\right)$ is the linear attenuation coefficient of XRF photons. Ang is the solid angle range covered by the detector from $\vec{r}_P$. $l_P(\vec{r})$ denotes the line on which the emitted XRF are collected by the detector.

Usually, XFCT image can be reconstructed by a maximum-likelihood expectation maximization (ML-EM) algorithm due to its high level Poisson noise. The formula of each iteration is expressed as

$$x_j^{(k+1)} = \frac{x_j^{(k)}}{\sum_{i=1}^{M} a_{ij}} \sum_{i=1}^{M} \frac{a_{ij} p_i}{\sum_{j'=1}^{N} a_{ij'} x_{j'}^{(k)}} \tag{4}$$

where a_{ij} is the coefficient of the imaging matrix which can be calculated from the XFCT geometry. i and j denote the i-th XRF photon beam and the j-th pixel of the reconstructed image, respectively. p_i is the measured XRF photon counts.

When the two fiducial markers locate at a different height above the detector, we have $B_z \neq B_z$.

III. EXPERIMENT RESULTS

Experiments were done on our SKYFI setup as showed in Fig. 2. A low-brilliance X-ray beam (150 kV, 3 mA) was generated using a conventional X-ray tube. The X-ray beam was collimated using lead plates in two directions to produce a fan beam. To reduce the total dose and scattering photons, a 0.4 mm Cu fiber was placed at the X-ray tube exit. A homemade PMMA (polymethyl methacrylate) phantom was set to rotate in precise steps using a computer-controlled motion stage, whereas the X-ray tube and the detectors were stationary. The third generation CT scanning mode was used with a rotational step of 1° over a full-scan. At each angle view, XFCT data emitted from the whole phantom illuminated using the full-field fan-beam were collected in 5 seconds by a linear photon counting detector array (eV3500, eV PRODUCTS, Saxonburg, PA). A 5 mm tungsten pinhole collimator was placed before the detector. This X-ray detector used a 3 mm CdZnTe (cadmium zinc telluride) semiconductor, 256 pixels at a 0.5 mm pixel pitch, and 5 adjustable energy thresholds. The detector was placed at a 90° angle to the incident X-ray beam to minimize the number of scattering photons entering the detector. Moreover, the same X-ray detector was repositioned behind the phantom along the beam direction to provide transmission spectral CT measurements and correct the attenuation. A PMMA phantom containing water and gadolinium solution insertions was prepared. The insertions consisted of air, water, and 1.7%, 0.39%, 0.62%, 0.82%, 0.99%, 1.5% (weight/volume) gadolinium solutions. The phantom dimension was 50 mm in diameter.

Fig.2. Photograph of the SKYFI imaging setup.

The K_α peak of gadolinium is located at 42.74 keV which was also the energy-bin center for XRF data acquisition. Figs. 3(a-d) are the XFCT reconstruction images with different energy-bin widths of 4, 5, 6 and 7 keV. The display window was [0 2%]w/v.

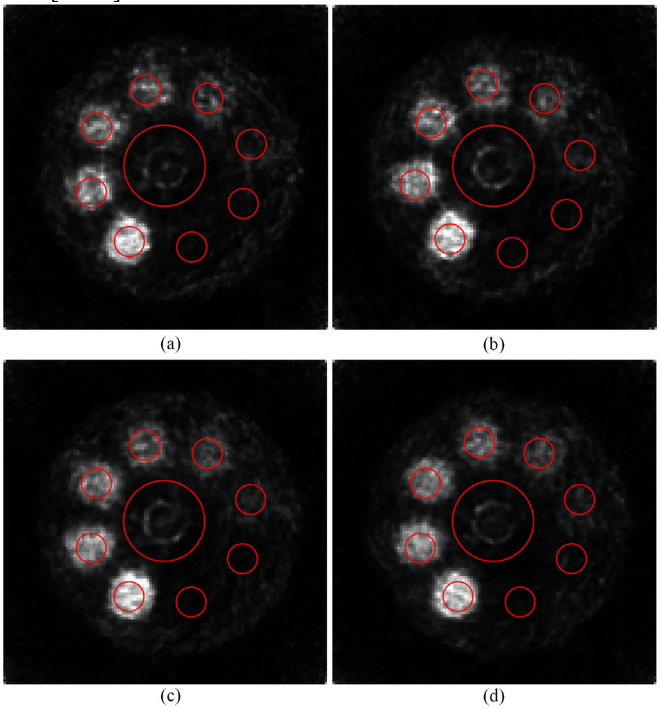

Fig.3. XFCT reconstruction images with different energy-bin widths.

To quantify the XFCT reconstructions in Fig. 3, we calculated the CNR between the mean value of gadolinium solutions and the standard deviation of water and air insertions. The results are shown in Table 1. After the scattering and attenuation correction, the XFCT image for 6 keV energy-bin has the highest CNR. And, 0.17% gadolinium solution can be distinguished.

Table.1 CNR comparisons among Figs 3(a-d).

Conc	0.17%	0.39%	0.62%	0.82%	0.99%	1.5%
Fig. 3(a)	3.00	11.57	17.71	24.40	30.59	48.69
Fig. 3(b)	4.30	11.91	20.03	27.12	32.88	50.82
Fig. 3(c)	6.17	15.42	23.96	34.99	44.87	65.92
Fig. 3(d)	3.35	8.63	15.34	18.43	23.11	35.82

Fig.4 shows the linear relationship between the gadolinium solution concentration and XFCT reconstruction value. Both the highly linear response (R^2=0.9982) and the characteristic passing through the zero point of XFCT with respect to the concentrations of contrast agents both suggest that XFCT is capable of quantitatively biomedical imaging and identifies a clear path toward for molecular imaging.

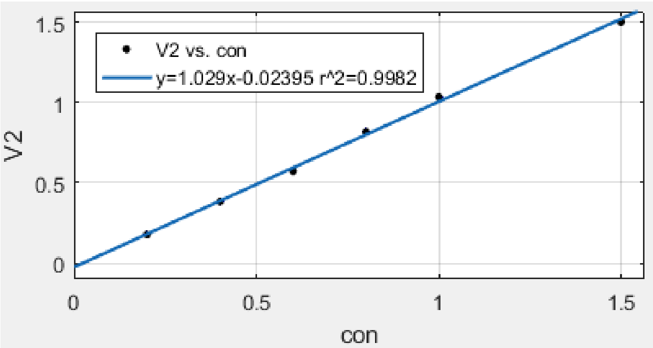

Fig.4. The linear relationship between the gadolinium solution concentration and XFCT reconstruction value.

IV. Discussion and conclusion

This paper presents the study of full-field, fan-beam XFCT using a conventional low-intensity X-ray tube and energy-resolved photon-counting detectors. Unlike the other rotation-and-translation scans of pencil beam cases, the XRF photons excited from full-filed fan-beam X-rays can be collected by passing through a tungsten pinhole collimator. Thus, XFCT scanning can be completed within 30 min using the third-generation CT geometry, which is much faster than other reported XFCT devices. Experimental results showed this full-field XFCT high sensitivity and accuracy in quantitative imaging. As a state-of-the-art result, last year Manohar et al. reported the first experimental result of XFCT on small animals. They obtained the distribution of gold NPS injected into a tumor-bearing mouse on their benchtop XFCT with a polychromatic X-ray tube [9]. Although they still used the first generation CT geometry leading to 1.5 hours for each XFCT slice and the detection limit of their system was only ~0.24 wt%, their results showed beyond all doubt the unique capabilities of benchtop XFCT for determination of the spatial distribution and concentration of nonradioactive NPs probes within the context of small animal or preclinical imaging. Therefore, we have reason to believe that this kind of full-field fan-beam XFCT is a promising modality for molecular imaging. Small animal XFCT experiment on this SKYFI system is under way.

References

[1] A. C. Kak and M. Slaney, Principles of Computerized Tomographic Imaging. Piscataway, NJ: IEEE Press, 1987.

[2] Wang G, Yu H Y, Man B D. “An outlook on x-ray CT research and development”, Med. Phys., 35(3): 1051- 1064, 2008.

[3] L. Li, Z. Q. Chen, W. X. Cong, et al. “Spectral CT modeling and reconstruction with hybrid detectors in dynamic-threshold-based counting and integrating modes”, IEEE Trans Med Imag, 34(3): 716-728, 2015.

[4] G. F. Rust, J. Weigelt, “X-ray fluorescent computer tomography with synchrotron radiation,” IEEE Trans. Nucl. Sci. 45(1), 75-88 (1998).

[5] G. Pratx, C. M. Carpenter, C. Sun, R. P. Rao, L. Xing, “Tomographic molecular imaging of x-ray-excitable nanoparticles,” Opt. Lett. 35(20), 3345–3347 (2010).

[6] S. K. Cheong, B. J. Jones, A.K. Siddiqi, F. Liu, N. Manohar, S. H. Cho, “X-ray fluorescence computed tomography (XFCT) imaging of gold nanoparticle-loaded objects using 110 kVp x-rays,” Phys. Med. Biol. 55(3): 647-662 (2010).

[7] M. Bazalova, Y. Kuang, G. Pratx, L. Xing, “Investigation of X-ray fluorescence computed tomography (XFCT) and K-Edge imaging,” IEEE Trans. Med. Imag. 31, 1620–1627 (2012).

[8] L. Li, Z. Q. Chen, G. Wang, et al. A tensor PRISM algorithm for multi-energy CT reconstruction and comparative studies, J. X-Ray Sci. Tech., 22: 147–163, 2014.

[9] N. Manohar, F. J. Reynoso, P. Diagaradjane, et al. Quantitative imaging of gold nanoparticle distribution in a tumor-bearing mouse using benchtop x-ray fluorescence computed tomography, Scientific Reports | 6:22079 | DOI: 10.1038/srep22079.

[10] Boisseau and L. Grodzins, “Fluorescence tomography using synchrotron radiation,” Hyperfine Interact. 33, 283–292 (1987).

[11] R. Cesareo and S. Mascarenhas, “A new tomographic device based on the detection of fluorescent X-rays,” Nucl. Instrum. Methods, vol. A277, pp. 669–672, 1989

[12] D. G. Lewis, “Optimization of a polarized source for in vivo x-ray fluorescence analysis of platinum and other heavy metals,” Phys. Med. Biol. 39, 197–206 (1994).

[13] T. Takeda, T. Maeda, T. Yuasa, et al., “Fluorescent scanning x-ray tomography with synchrotron radiation,” Rev. Sci. Instrum., vol. 66, no. 2, pt. 2, pp. 1471–1473, Feb. 1995.

[14] P. A. Ali, A. F. Al-Hussany, C. A. Bennett, D. A. Hancock, and A. M. El-Sharkawi, “Plane polarized x-ray fluorescence system for the in vivo measurement of platinum in head and neck tumours,” Phys. Med. Biol. 43, 2337–2345 (1998).

[15] R. Schmitz, A. Bingölbali, A. Hussain, and C. A. MacDonald, “Development of polarized and monochromatic x-ray beams from tube sources,” Proc. SPIE 7077, 70770Y-1–70770Y-8 (2008).

[16] L. J. Meng, N. Li, and P. J. La Rivière, “X-ray fluorescence tomography using emission tomography systems,” IEEE Trans. Nucl. Sci. 58, 3359–3369 (2011).

[17] B. Deng, G. Du, G. Zhou, et al., “3D elemental sensitive imaging by full-field XFCT,” Analyst 140(10), 3521-3525 (2015)

[18] S.K. Cheong, B. J. Jones, A.K. Siddiqi, F. Liu, N. Manohar, S. H. Cho, “X-ray fluorescence computed tomography (XFCT) imaging of gold nanoparticle-loaded objects using 110 kVp x-rays,” Phys. Med. Biol. 55(3): 647-662 (2010).

[19] B. L. Jones and S. H. Cho, “The feasibility of polychromatic cone-beam x-ray fluorescence computed tomography (XFCT) imaging of gold nanoparticle-loaded objects: A Monte Carlo study,” Phys. Med. Biol. 56, 3719–3730 (2011).

[20] M. Bazalova, Y. Kuang, G. Pratx, L. Xing, “Investigation of X-ray fluorescence computed tomography (XFCT) and K-Edge imaging,” IEEE Trans. Med. Imag. 31, 1620–1627 (2012).

[21] P. L. Riviere, D. Billmire, P. Vargas, et al., “Penalized-likelihood image reconstruction for x-ray fluorescence computed tomography,” Opt. Eng. 45(7), 077005 (2006).

[22] G. Pratx, C. M. Carpenter, C. Sun, L. Xing, “X-ray luminescence computed tomography via selective excitation: A feasibility study,” IEEE Trans. Med. Imag. 29(12), 1992–1999 (2010).

[23] G. Fu, L. J. Meng, P. Eng, et al., “Experimental demonstration of novel imaging geometries for x-ray fluorescence computed tomography,” *Med. Phys.* **40**(6), 061903 (2013).

[24] N. Manohar, B. L. Jones, S. H. Cho, “Improving x-ray fluorescence signal for benchtop polychromatic cone-beam x-ray fluorescence computed tomography by incident x-ray spectrum optimization: A Monte Carlo study,” Med. Phys. 41(10), 101906 (2014).

[25] H. M. Hertz, J. C. Larsson, U. Lundstrom, et al., “Laboratory x-ray fluorescence tomography for high-resolution nanoparticle bio-imaging,” Opt. Lett. 39(9), 2790-2793 (2014).

[26] A. Groll, J. George, P. Vargas, P. L. Riviere, L. J. Meng, “Element Mapping in Organic Samples Utilizing a Benchtop X-Ray Fluorescence Emission Tomography (XFET) System,” IEEE Trans. Nucl. Sci. 62(5), 2310-2317 (2015).

[27] Y. Kuang, G. Pratx, M. Bazalova, B.W. Meng, J.G. Qian, L. Xing, “First demonstration of multiplexed x-ray fluorescence computed tomography (XFCT) imaging,” IEEE Trans. Med. Imag. 32(2), 262-267 (2013).

[28] L. Li, S. Y. Zhang, R. Z. Li, et al., “Simultaneous X-ray fluorescence and K-edge CT imaging with photon-counting detectors,” *Proc. SPIE*. **9967**, 99670F (2016).

[29] R. Z. Li, L. Li, Z. Q. Chen. Feasible Energy Calibration for Multi-threshold Photon-counting Detectors Based on Reconstructed XRF Spectra, IEEE Trans. Nucl. Sci., DOI: 10.1109/TNS.2016.2645721